Galaxy Gas Fractions, Characteristic Mass Scales, and the RESOLVE Survey

Sheila J. Kannappan* and Lisa H. Wei†

*Department of Physics and Astronomy, University of North Carolina, Chapel Hill, NC 27599
†Department of Astronomy, University of Maryland, College Park, MD 20742

Abstract. We relate various measures of galaxy mass, using new data for the Nearby Field Galaxy Survey (NFGS). (1) Key mass and velocity transition scales previously identified in the literature are put on a common scale, indicating that the "bimodality mass" at $M_* \sim$ a few $\times 10^{10} M_{sun}$ corresponds to $V \sim 190$ km/s and is distinct from the gas-richness "threshold mass" at $M_* \sim$ several $\times 10^9 M_{sun}$, which roughly corresponds to $V \sim 120$ km/s. This value of the threshold mass is based on ionized gas detections and HI data for the NFGS, a smaller but statistically better-defined sample than that used for the original identification of the gas-richness threshold. (2) We argue that *R*-band light is the best available photometric tracer of dynamical mass over a wide range in mass and morphology, whereas *U* and *K* more closely trace just gas and stellar mass, respectively. The NFGS confirms evidence for an incredibly tight correlation between $U-K$ color and atomic-gas–to–stellar mass ratio $M_{atomic\ gas}/M_{stars}$, yielding rms scatter $\sigma \simeq$ a factor of 2 (FWHM $\simeq$ a factor of 5) in $M_{atomic\ gas}/M_{stars}$. (3) We examine why *U* band light from recent star formation correlates so well with *atomic* gas, when stars form in *molecular* gas. We propose that time-averaged molecular-to-atomic gas ratios stay within a factor of $\sim$5 range over the 100+ Myr timescales to which the *U* band is sensitive, due to episodic gas inflow events that replenish molecular gas, and we show evidence for such events. Finally, we consider the implications of these results for the design of the RESOLVE Survey, a mass census of the $z = 0$ cosmic web.

Keywords: galaxy evolution, cosmic web
PACS: 98.62.-g, 98.65.-r

1. INTRODUCTION

The evolution of galaxies appears increasingly inseparable from that of the cosmic web in which they live. Not only does merging build structure on all scales from dwarf galaxies to superclusters, but recent research suggests that cold gas accretion onto galaxies may arrive via cosmic flows along the large-scale filaments defined by galaxy clustering. The time is ripe for a deep census of a large, contiguous volume of the $z = 0$ cosmic web, tracing multiple interconnected environments and their dynamics while surveying the gas, stellar, and dark matter content of the galaxies embedded within. Key science goals include measuring the galaxy mass function and its relationship to the halo mass function, determining merger rates as a function of mass ratio and environment, and analyzing the physics of disk building and rebuilding in relation to local and global environment. Here we present results from a precursor survey that have direct relevance to survey design for a mass census of the $z = 0$ cosmic web. We then introduce the RESOLVE (REsolved Spectroscopy Of a Local VolumE) Survey, which will perform this census in an ambitious multiwavelength program building on the rich treasury of data available in equatorial regions accessible to both northern and southern telescopes.

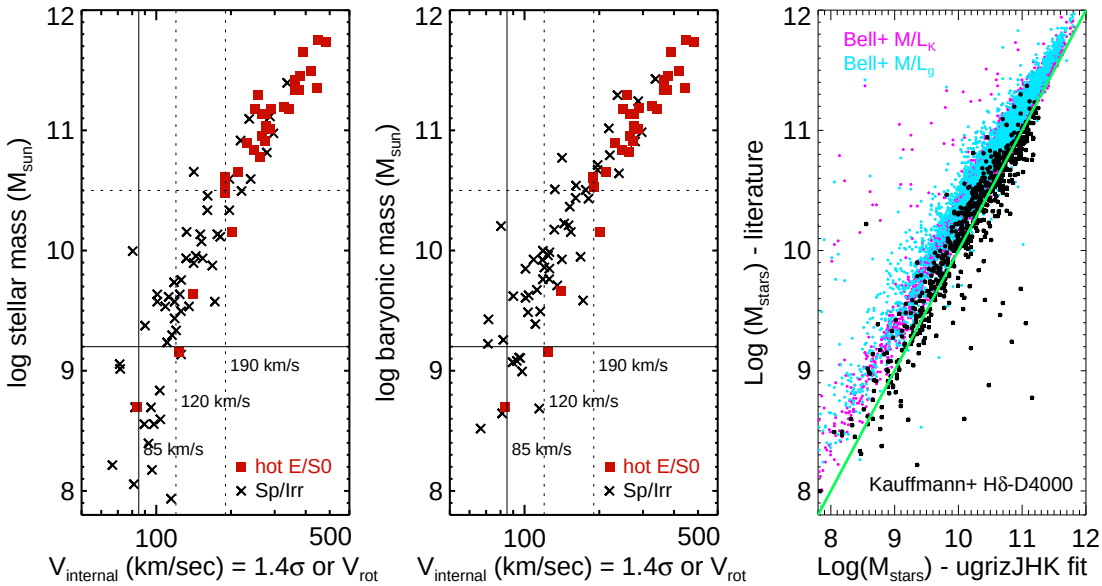

FIGURE 1. Correspondence of key mass and velocity scales in the Nearby Field Galaxy Survey (NFGS, [1]). *Left two panels.* Mass–internal velocity relations using (a) stellar masses computed by fitting SEDs and spectra (§ 2.1) and (b) baryonic masses computed by adding atomic gas masses based on 21 cm line data with a 1.4× He correction factor. Dashed lines mark 120 km/s, the transitional velocity scale identified by [2], and 190 km/s, corresponding to the bimodality mass $M_b \sim 3\times10^{10}M_{sun}$ found by [3]. The solid line marks the approximate low-velocity limit of the RESOLVE Survey. Internal velocity dispersions σ are scaled as described in [4]; we do not plot E/S0s whose dispersions may be low due to substantial rotation support (but see Fig. 5). *Right panel.* Comparison of stellar mass estimates for the sample of [3], illustrating that masses derived by the SED-fitting method used here are close to those of [3], with both sets of masses ∼1.5× smaller than those based on the color–M_*/L calibrations of [5].

2. GUIDANCE FROM A PRECURSOR SURVEY

The Nearby Field Galaxy Survey (NFGS, [1]) is a broadly representative $z = 0$ survey spanning all environments and morphologies. Its luminosity distribution is roughly proportional to the $z = 0$ luminosity function, within the constraints of a magnitude-limited parent survey (the CfA1 Redshift Survey). With <200 galaxies and no contiguous environmental coverage, the NFGS offers little insight into the cosmic web, but its broad characteristics make it ideal for analyzing design constraints for more ambitious surveys.

2.1. Key mass and velocity scales

Figs. 1 and 2 illustrate the relationship between the bimodality mass at $\sim3\times10^{10}M_{sun}$ reported by [3], the sharp transition velocity at 120 km/s reported by [2], and the atomic gas-richness threshold mass reported by [6]. Careful matching of stellar mass estimation techniques (Fig. 1) and more precise identification of the gas-richness threshold mass using the NFGS (Fig. 2) reveal that these scales are not all identical. The gas-richness threshold mass M_t occurs near $\log M_* \sim 9.5$–9.7 and roughly matches the 120 km/s

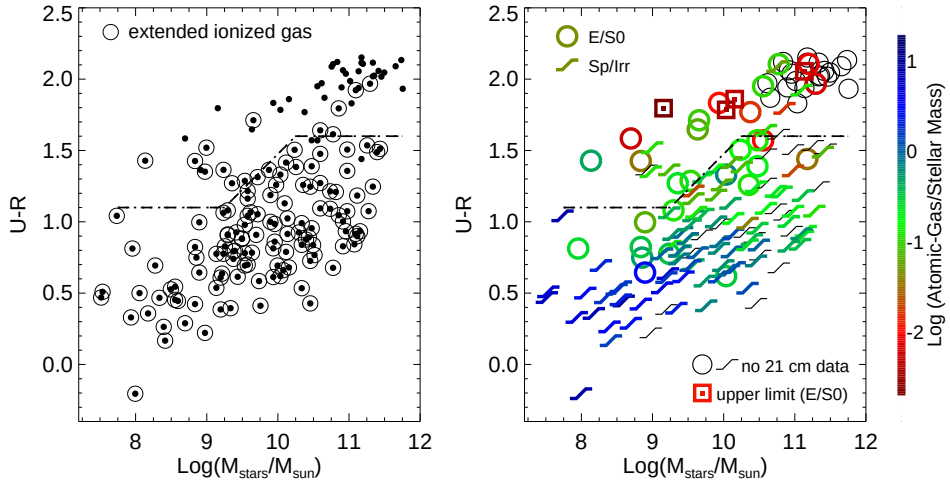

FIGURE 2. Evidence for a gas-richness threshold in stellar mass at $\log M_t \sim 9.5$–9.7, i.e., near $V \sim 120$ km/s, in the Nearby Field Galaxy Survey (confirming prior evidence based on a less statistically robust sample drawn from SDSS, 2MASS, and HyperLeda; see [6]). *Left panel.* Detections of spatially extended ionized gas emission (circles) within the NFGS, shown distributed in $U-R$ color vs. stellar mass. Red-sequence detections sharply increase below M_t, although all galaxies were observed with comparable sensitivity. *Right panel.* $M_{atomic\,gas}/M_{stars}$ (color coded as shown by the color bar at right), again distributed in $U-R$ color vs. stellar mass. Thin black symbols represent NFGS galaxies not yet observed at 21 cm. The data show generally higher gas content below M_t (with substantial scatter on the red sequence).

velocity reported to mark the onset of efficient star formation and narrow dust lanes [2]. The bimodality mass M_b occurs closer to $V \sim 190$ km/s, separating regimes of old vs. young stellar populations and spheroid- vs. bulge-dominated morphology, as reported by [3]. Interestingly, E/S0 galaxies appear on the *blue* sequence below M_b (see [7] for a discussion of possible disk regrowth in this population).

These results rely on updated stellar mass estimation techniques. We adapt the code of [4], which fits SEDs and spectra with a grid of models and bins the model likelihoods over stellar masses, then gives the median of this distribution as the mass estimate. This procedure is sensitive to the number of models with a given mass, so we have modified the model grid used by [4] to sample possible masses more realistically. Each model combines a base simple stellar population (SSP) with either a second base SSP or a "recent-burst" SSP (all from [8]). The base SSPs have one of 13 ages distributed roughly linearly (1.4, 2.5, 3.5... 13.5 Gyr), while the recent-burst SSPs have one of four ages distributed roughly logarithmically (25 Myr, 290 Myr, 640 Myr, 1 Gyr). We generate mixed-age pairs with 1%, 2%, 4%, 8%, 16%, 32%, and 64% of the mass in the younger SSP, and we also allow single SSP models. The likelihood for any model with a recent-burst SSP is divided by 4 to account for the overdensity of SSPs with ages below 1 Gyr. Models are generated with three metallicities (0.4, 1, 2.5$Z_\odot$), which can differ for each SSP, and six reddenings $\tau_{V,gas}$ (0, 0.24, 0.48, 0.72, 0.96, 1.2), which are applied to the combined model. We fit to *UBRJHK* + integrated spectrophotometry for the NFGS, and to *ugrizJHK* for the sample of [3] (Fig. 1).

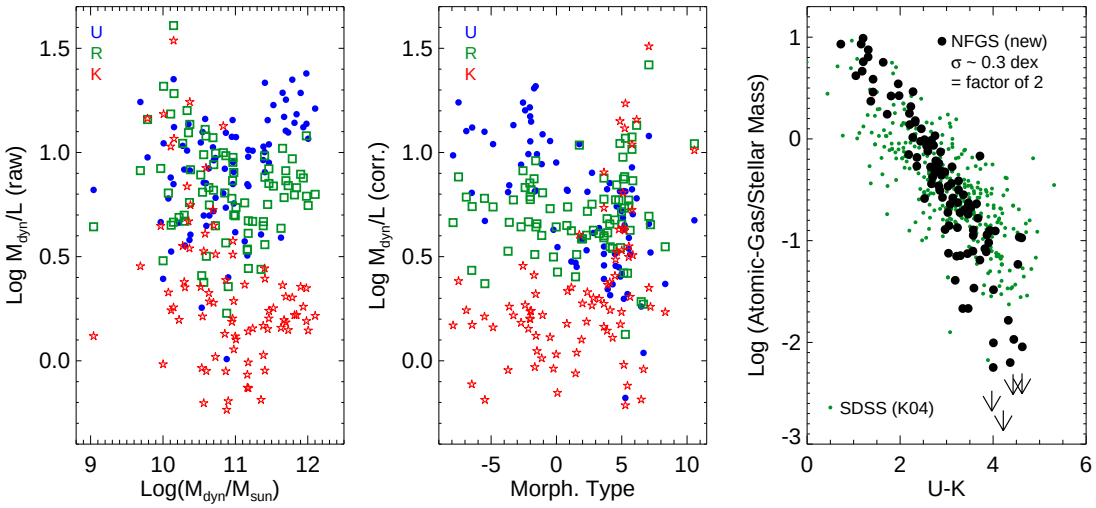

FIGURE 3. *Left panels.* Dynamical mass to light ratio M_{dyn}/L in U, K, and R as a function of M_{dyn} and morphological type for the NFGS. Internal extinction corrections and K-corrections are applied in the middle but not the left panel. Small random offsets are added to the types in the middle panel for clarity. Dynamical masses are computed as in [4]. *Right panel.* $M_{atomic\ gas}/M_{stars}$ vs. U-K for the NFGS (large dots), with remarkably tight scatter. For comparison, the relation of [6] based on lower-quality SDSS data is also shown (small dots), with $u-K$ shifted to underlie $U-K$ near the middle and stellar masses scaled down to match the current mass scale (masses in [6] are based on [5]; see Fig. 1 for a comparison).

2.2. Which light best traces mass?

Fig. 3 demonstrates empirically that R-band luminosity is the best available photometric tracer of dynamical mass for all morphological types, for dynamical masses down to $\sim 10^{10} M_{sun}$ or slightly below. Notably, K-band light is *not* a good tracer of dynamical mass for late-type and/or low-mass galaxies, simply because stellar and dynamical masses diverge for these gas-rich galaxies, and K-band light seems to track primarily the stellar component. However, U-band light tracks HI content closely, especially when normalized to the K band. Thus $U-K$ correlates with $M_{atomic\ gas}/M_{stars}$ and we see opposite trends for M_{dyn}/L_U and M_{dyn}/L_K, especially after extinction and K-corrections are applied (compare left and middle panels of Fig. 3).

2.3. Linking atomic and molecular gas

As seen in Fig. 3, the scatter in the $U-K$ vs. $M_{atomic\ gas}/M_{stars}$ correlation is extremely tight: $\sigma \sim 0.3$ dex = factor of 2 (FWHM = factor of 5) for $U-K$ from 1–3, beyond which the relation broadens. (The relation is tighter than that reported by [6] due to internal extinction corrections, higher-quality U-band data, improved stellar mass estimation, and better HI data, including new GBT data to be published in [9].) Interpreting $U-K$ as a measure of the ratio of recent to past-averaged star formation – i.e., a 100+ Myr time-average of the Scalo b parameter – we infer that long-term star forma-

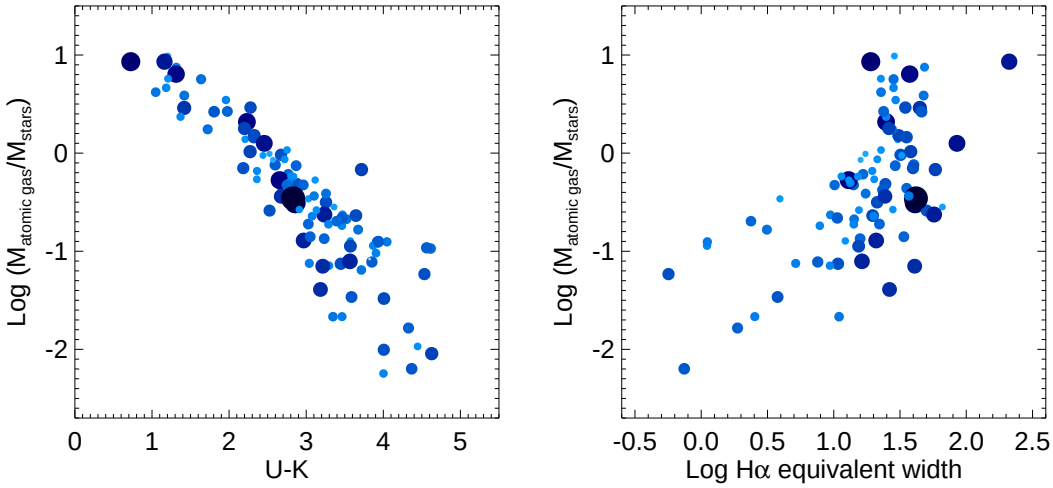

FIGURE 4. $M_{atomic\ gas}/M_{stars}$ vs. *(a)* $U-K$ and *(b)* EW(Hα) for the NFGS. Larger/darker symbols indicate more blue-centered color gradients, using the $\Delta(B-R)_{\rm corr}$ parameter defined by [10]. See § 2.3.

tion closely tracks the HI reservoir. Since stars form in *molecular* gas, and instantaneous molecular-to-atomic gas ratios can vary widely, we suspect that the tight scatter in Fig. 3 implies that long-term-averaged H_2:HI ratios are smoothed on timescales $<$100 Myr.

Fig. 4 shows evidence that this smoothing process may be linked to episodic gas inflow events that resupply molecular gas and fuel central star formation. We compare $M_{atomic\ gas}/M_{stars}$ vs. two different Scalo *b* tracers: $U-K$ color, sensitive to star formation over the last 100+ Myr, and global EW(Hα), sensitive to star formation in the last 5–10 Myr. Residuals in the EW(Hα) plot are much larger and correlate with "blue-centeredness" (dot color and size), a sensitive tracer of small central bursts. Following [10], we measure blue-centeredness using the $\Delta(B-R)_{\rm corr}$ parameter, which equals the difference between the half-light and outer-disk colors "corrected" by subtracting the mean color difference for galaxies of the same luminosity. From [10], we know that $\Delta(B-R)_{\rm corr}$ correlates with evidence of minor mergers and interactions, which may drive gas inflow. We are working to obtain CO data for this sample to test the idea that H_2:HI ratios vary cyclically with $\Delta(B-R)_{\rm corr}$, EW(Hα), and/or stellar line diagnostics.

3. THE RESOLVE SURVEY

The above results bear on survey design for the RESOLVE (REsolved Spectroscopy Of a Local VolumE) Survey, a mass census of the $z=0$ cosmic web with the SOAR telescope. At the heart of the survey is high spatial- and spectral-resolution spectroscopy to measure internal kinematics and stellar population diagnostics. RESOLVE has been selected in SDSS equatorial strips that will soon have ALFALFA HI data (or upper limits), UKIDSS NIR imaging, and GALEX MIS UV imaging. We are working on "cheap" diagnostics of H_2:HI ratios (§ 2.3), and RESOLVE will also be accessible to ALMA. The initial sample derives from the SDSS redshift survey, whose limit at $r\sim17.77$ represents

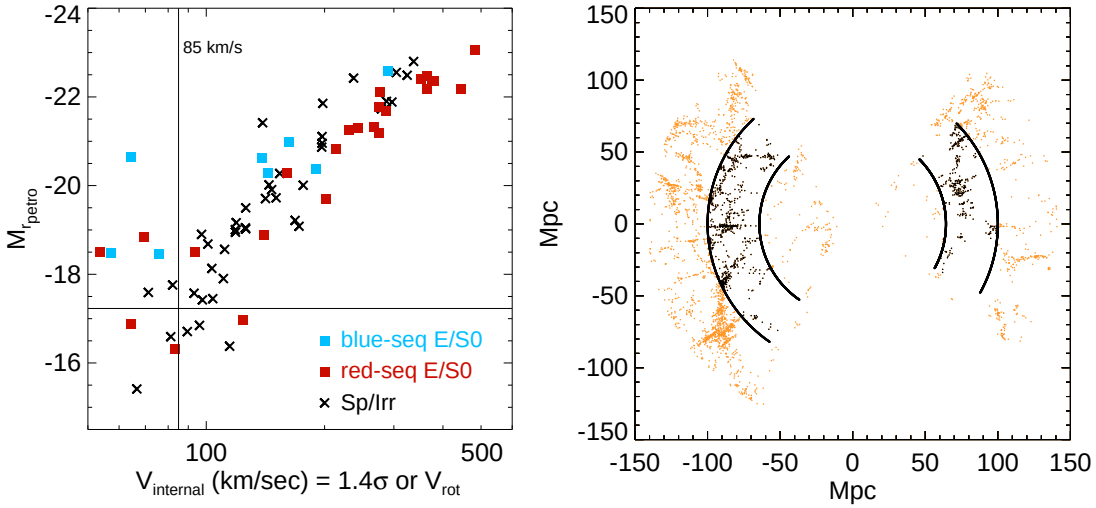

FIGURE 5. *Left panel.* Absolute *r*-band magnitude vs. internal velocity for NFGS galaxies with SDSS data. The SDSS redshift survey limit corresponds to $M_r = -17.23$ at the far side of the RESOLVE Survey volume (7000 km/s), so we adopt this magnitude limit at all redshifts in the initial selection, yielding a velocity cutoff at ∼85 km/s. *Right panel.* The initial RESOLVE sample drawn from SDSS DR6 [11].

an approximate dynamical mass limit well below the interesting mass scales at M_b and M_t (compare Figs. 1, 3, 5). To improve completeness for low surface brightness galaxies above the RESOLVE mass limit, we will identify objects missed by the SDSS redshift survey using HI redshifts from ALFALFA as well as spectroscopic redshifts from SOAR, targeted based on SEDs. The combined data set will provide gas, stellar, and dynamical masses for both galaxies and larger structures in a volume spanning multiple interconnected environments, with excellent prospects as a target region for next-generation surveys at other wavelengths.

ACKNOWLEDGMENTS

We thank S. Vogel and A. Baker for permission to show new GBT HI data from [9].

REFERENCES

1. R. A. Jansen, and S. J. Kannappan, *Ap&SS* **276**, 1151–1159 (2001).
2. J. J. Dalcanton, P. Yoachim, and R. A. Bernstein, *ApJ* **608**, 189–207 (2004).
3. G. Kauffmann et al., *MNRAS* **341**, 54–69 (2003).
4. S. J. Kannappan, and E. Gawiser, *ApJ* **657**, L5–L8 (2007).
5. E. F. Bell, D. H. McIntosh, N. Katz, and M. D. Weinberg, *ApJ Supp* **149**, 289–312 (2003).
6. S. J. Kannappan, *ApJ* **611**, L89–L92 (2004).
7. S. J. Kannappan, J. M. Guie, and A. J. Baker, *AJ, submitted* (2008).
8. G. Bruzual, and S. Charlot, *MNRAS* **344**, 1000–1028 (2003).
9. L. H. Wei, S. J. Kannappan, S. N. Vogel, and A. J. Baker, *in preparation* (2008).
10. S. J. Kannappan, R. A. Jansen, and E. J. Barton, *AJ* **127**, 1371–1385 (2004).
11. J. K. Adelman-McCarthy et al., *ApJ Supp* **175**, 297–313 (2008).